Two types of photoluminescence blinking revealed by single quantum dot spectroelectrochemistry

Supplementary Information

I. Statistical scaling and rate equations

We estimate the radiative and non-radiative decay rates of neutral and charged excitons using a statistical scaling, which considers the number of recombination pathways that lead to the final carrier configuration[1,2]. The radiative decay of the neutral exciton is denoted γ_r. We introduce a non-radiative decay rate γ_{nr} to account for processes such as energy transfer to the conductive ITO[3]. We denote the constant, which characterizes the rate of a single pathway in Auger recombination as γ_A. If we account for all possible carrier configurations and recombination channels in the state i with n_e electrons and n_h holes, we obtain the following scaling for the radiative rate γ_r^i and Auger decay rate γ_A^i.

$$\gamma_r^i = n_e\, n_h\, \gamma_r \qquad \text{and} \qquad \gamma_A^i = n_e\, n_h\, (n_e + n_h - 2)\, \gamma_A \qquad (1)$$

Applying these expressions to the radiative rates of the neutral, singly- and doubly-charged excitons, we obtain (we assume the presence of excess negative charges):

$$\gamma_r^0 = \gamma_r \qquad \gamma_r^- = 2\gamma_r \qquad \gamma_r^{2-} = 3\gamma_r. \qquad (2)$$

The corresponding rates of nonradiative processes are:

$$\gamma_{nr}^0 = \gamma_{nr} \qquad \gamma_{nr}^- = \gamma_{nr} + 2\,\gamma_A \qquad \gamma_{nr}^{2-} = \gamma_{nr} + 6\,\gamma_A \qquad (3)$$

The total decay rate of state i is: $\gamma_{tot}^i = \gamma_r^i + \gamma_{nr}^i$. It directly relates to the PL lifetime measured experimentally: $\tau_{PL}^i = 1/\gamma_{tot}^i$. The quantum yield is then given by:

$$QY^i = \gamma_r^i / \gamma_{tot}^i \qquad (4)$$

The ratios of the QYs on neutral and charged excitons are not dependent on the scaling assumed for the non-radiative rates and can be presented as:

$$QY^-/QY^0 = 2\,(\gamma_{tot}^0 / \gamma_{tot}^-) = 2\,(\tau_{PL}^- / \tau_{PL}^0) \qquad (5)$$

$$QY^{2-}/QY^- = 3/2\,(\gamma_{tot}^- / \gamma_{tot}^{2-}) = 3/2\,(\tau_{PL}^{2-} / \tau_{PL}^-) \qquad (6)$$

Since the measured PL intensity is proportional to the QY, we can easily verify the validity of these equations for the nanocrystal shown in Fig. 2-3. On the basis of the measured lifetimes ($\tau_{PL}^0 = 24$ ns, $\tau_{PL}^- = 5$ ns, and $\tau_{PL}^{2-} = 2$ ns), we expect the following relationships between the PL intensities of different states:

$$I_{PL}^- / I_{PL}^0 = 2*5/24 \approx 0.4 \quad \text{and} \quad I_{PL}^{2-} / I_{PL}^- = 3/2*(2/5) = 0.6$$

The measured intensities are in excellent agreement with the predicted values:

$$I_{PL}^-/I_{PL}^0 \approx 30/85 \approx 0.35 \quad \text{and} \quad I_{PL}^{2-}/I_{PL}^- \approx 18/30 = 0.6.$$

We can now use the above scaling to extract the three unknown rates γ_A, γ_r, and γ_{nr} from the three accessible experimental quantities γ_{tot}^0, γ_{tot}^-, and γ_{tot}^{2-} by solving a system of three equations. This yields:

$$\gamma_A = \gamma_{tot}^0 - 2\,\gamma_{tot}^- + \gamma_{tot}^{2-} \qquad (7a)$$
$$\gamma_r = -2\,\gamma_{tot}^0 + 3\,\gamma_{tot}^- - \gamma_{tot}^{2-} \qquad (7b)$$
$$\gamma_{nr} = 3\,\gamma_{tot}^0 - 3\,\gamma_{tot}^- + \gamma_{tot}^{2-} \qquad (7c)$$

For the nanocrystal shown in Figs. 2-3, we obtain $\gamma_A \approx 0.14$ ns^{-1}, which allows us to calculate the Auger lifetime of the negative trion (X$^-$):

$$\tau_A^- = 1/(2\gamma_A) \approx 3.5 \text{ ns}$$

Similarly, we obtain: $\tau_{rad} = 60$ ns, $\tau_{nr} = 40$ ns, and $\tau_A^{2-} = 1/(6\gamma_A) \approx 1.2$ ns. As expected, the decay of the neutral exciton is dominated by non-radiative energy transfer to the ITO substrate. The PL quantum yield we calculate here is $QY^0 \approx 0.4$.

II. Simulated Fluorescence Lifetime - Intensity Distribution (FLID)

Within the framework described above, we can establish a relationship between the PL intensity, I_{PL}, and the average PL lifetime, τ_{avg}, in the regime of A-type blinking, for which we observe direct intensity – lifetime correlations. In this case, charge fluctuations and associated Auger quenching is assumed to be the dominant cause of intensity and lifetime variations. Here, we focus on fluctuations where X^0 and X$^-$ are primarily involved. For each time bin, the PL decay curve is fitted to a bi-exponential function:

$$A_0 \exp(-t/\tau_0) + A_1 \exp(-t/\tau_1) \quad \text{with} \quad \tau_0 \equiv \tau_{PL}^0 \text{ and } \tau_1 \equiv \tau_{PL}^-.$$

The ratio of the coefficients A_0 and A_1 gives the relative contributions of X^0 and X$^-$ to the measured PL, reflecting the portions of time spent by the nanocrystal in the X^0 and the X$^-$ states within each bin. Without loss of generality, we assume that $A_0 + A_1 = 1$. The PL intensity is given by:

$$I_{PL} = A_0\,I_{PL}^0 + A_1\,I_{PL}^1 \text{ with } I_{PL}^1 \equiv I_{PL}^- \qquad (8)$$

On the other hand, the average lifetime plotted in the color maps is defined as[a]:

---

[a] Using the alternative definition, $\tau_{avg} = (A_0\,\tau_0 + A_1\,\tau_1)/(A_0 + A_1)$, does not affect the results of this paper.

$$\tau_{avg} = (A_0 \tau_0^2 + A_1 \tau_1^2)/(A_0 \tau_0 + A_1 \tau_1) \qquad (9)$$

After simple arithmetic we obtain:

$$I_{PL} = I_{PL}^1 + (I_{PL}^1 - I_{PL}^0) \cdot \tau_1 / (\tau_1 - \tau_0) \cdot (\tau_1 - \tau_{avg}) / (\tau_{avg} - \tau_1 - \tau_0), \qquad (10)$$

where the values of I_{PL}^1, I_{PL}^0, τ_1, and τ_0 are taken from the experiment. This is the equation that we use to calculate the FLIDs shown as solid white lines in color plots of Figs. 3 and 4a. An important point is that in this analysis we do not use any adjustable parameters.

III. Effects of nanocrystal-to-nanocrystal variability on blinking behaviors

We would like to point out that we observe a large variability in the values of the X$^-$ charging potential from sample to sample, and from nanocrystal to nanocrystal within the same sample. Whereas a few nanocrystals do not show any signatures of charge injection, the electrochemically active nanocrystals typically show a behavior, which is consistent with charging at a potential ranging from $V = $ -0.5 to $V = $ -1.5 V. Such variability points to inhomogeneities of the ITO surface and variations in nanocrystal properties (e.g., shell thickness and/or surface coverage with ligands). This finding has significant implications for the interpretation of results observed in ensemble studies, in which the differences between individual nanocrystals are not resolved.

We now discuss the reasons for the difference in blinking characteristics between individual nanocrystals within the same sample in our experiments, and more generally, for the diversity of behaviors reported in the literature. In particular, we propose an explanation for the predominance of either A- or B-type blinking in a nanocrystal at neutral potential.

One parameter, which presumably determines the frequency and type of blinking events observed in a given nanocrystal, is the density of surface states and their nature. Yet, even if all nanocrystals have similar density, identity, and energy distribution of surface states, we still expect substantial variability in blinking depending on the alignment between the nanocrystal energy levels and the substrate Fermi energy. We believe that in our samples, inhomogeneity of the ITO layer (dopant concentration, thickness, roughness, etc.) is the primary cause of variations, but surface ligand coverage as well as the local chemical environment could also play an important role.

Referring to Fig. 4b, two typical situations are possible at neutral potential. If the Fermi level (E_F) at 0 V falls below the energy of the recombination centers (E_R), B-type blinking will be predominantly observed. Alternatively, when the band alignment at $V = 0$ V is such that E_F lies close to the $1S_e$ energy, the nanocrystal will be particularly prone to random charging and discharging and would mainly exhibit A-type blinking, as in the example shown in Fig. 3.

### IV. Relation to previous literature observations

PL Quantum Yields of ON and OFF states. One reason for challenging the "charging model" of PL intermittency has been observations that the QY of the OFF state can be much lower than the QY of a charged exciton (see, for example, Ref. 4). However, while being not consistent with

blinking due to charging (A-type blinking), these results can be rationalized if we invoke B-type blinking. Specifically, our findings indicate that B-type blinking dominates in thin-shell nanocrystals and, therefore, is likely a dominant blinking mechanism in standard core-only CdSe and core-shell CdSe/ZnS NQDs studied in earlier reports. In the case of B-type blinking, the QY of the OFF state is unrelated to the charged exciton Auger lifetime. Instead, it is defined by the rate of hot-carrier trapping compared to the carrier cooling rate. As a result, it can be much lower than the QY of a trion state, as observed in Ref. 4 for example.

PL dynamics in the OFF state. Another challenge for the "charging model" has been associated with the measurements of PL dynamics in the OFF state that seemed inconsistent with the Auger decay of charged excitons (e.g., did not exhibit the size dependence typical of Auger recombination; Ref. 5). These observations can also be explained by the model of B-type blinking. As discussed in the main text and illustrated in Fig. 4b, the B-type OFF periods may be accompanied by positive charging of the nanocrystal core. Moreover, we measure clear signatures of this charging in PL dynamics, as we show in Supplementary Fig. 5. If the charging during OFF periods remains insignificant then the measured PL decay is defined by the neutral exciton lifetime. On the other hand, if the role of charging is increased, the PL dynamics will be a superposition of neutral exciton and positive trion decays. The relative amplitude of the trion-related fast component and the *apparent* PL lifetime (e.g. the *1/e* decay time in Ref. 5) will strongly depend on the probability of photocharging, and hence, properties such as ligand coverage, identity of ligand species and the local environment. Thus, dot-to-dot variations in the degree of photocharing during OFF periods can lead to a wide spread of corresponding PL decay times from those of a neutral exciton to a positive trion. These considerations may explain both the appearance of fast PL decay during B-type OFF periods as well as the lack of any systematic size dependence for the fast PL component.

References

1   McGuire, J. A., Joo, J., Pietryga, J. M., Schaller, R. D. & Klimov, V. I. New aspects of carrier multiplication in semiconductor nanocrystals. *Acc. Chem. Res.* **41**, 1810-1819, (2008).
2   Klimov, V. I., McGuire, J. A., Schaller, R. D. & Rupasov, V. I. Scaling of multiexciton lifetimes in semiconductor nanocrystals. *Phys. Rev. B* **77**, 195324, (2008).
3   Jha, P. P. & Guyot-Sionnest, P. electrochemical switching of the photoluminescence of single quantum dots. *J. Phy. Chem. C* **114**, 21138-21141, (2010).
4   Zhao, J., Nair, G., Fisher, B. R. & Bawendi, M. G. Challenge to the charging model of semiconductor-nanocrystal fluorescence intermittency from off-state quantum yields and multiexciton blinking. *Phys. Rev. Lett.* **104**, 157403, (2010).
5   Rosen, S., Schwartz, O. & Oron, D. Transient fluorescence of the off state in blinking CdSe/CdS/ZnS semiconductor nanocrystals is not governed by auger recombination. *Phys. Rev. Lett.* **104**, 157404, (2010).
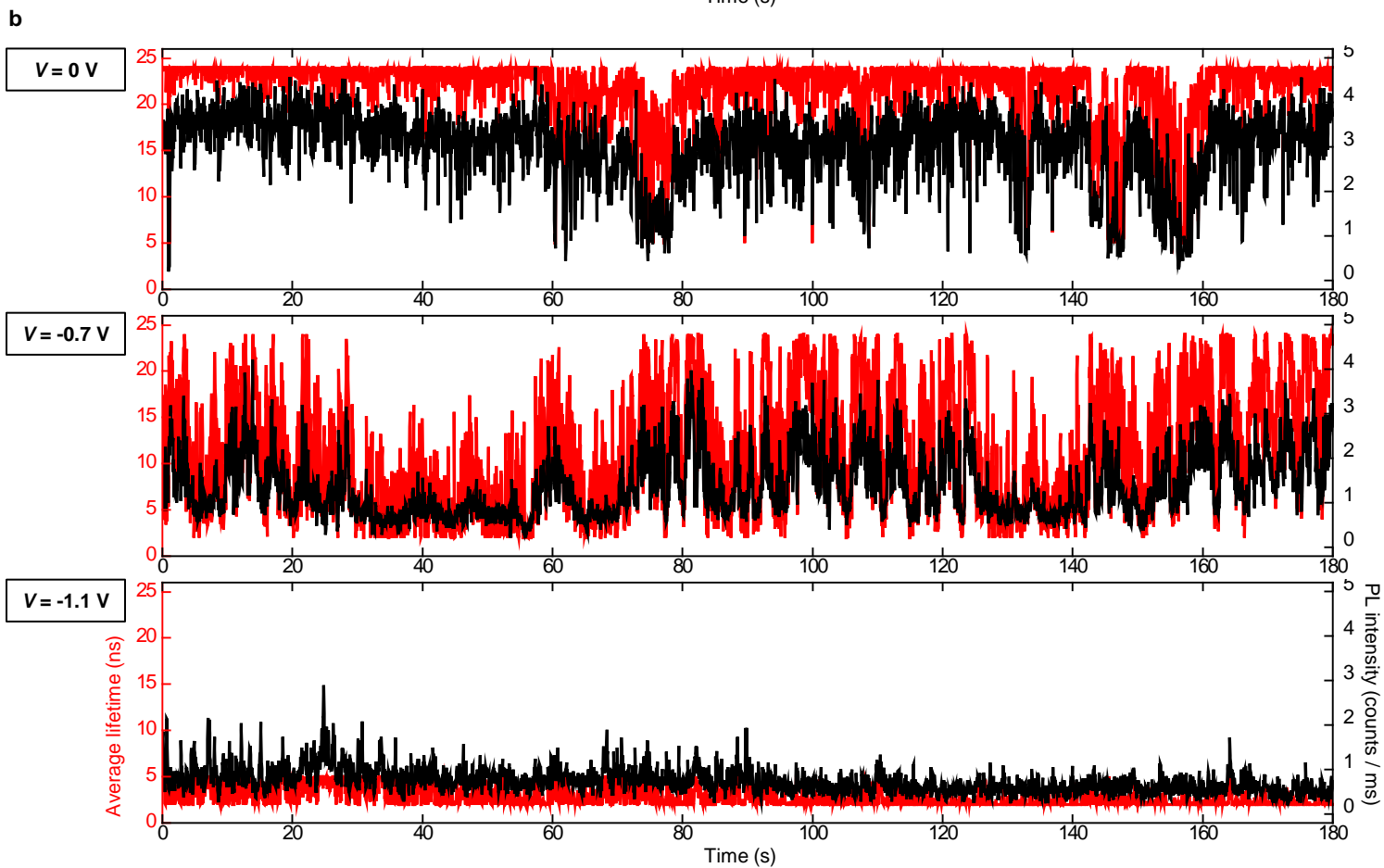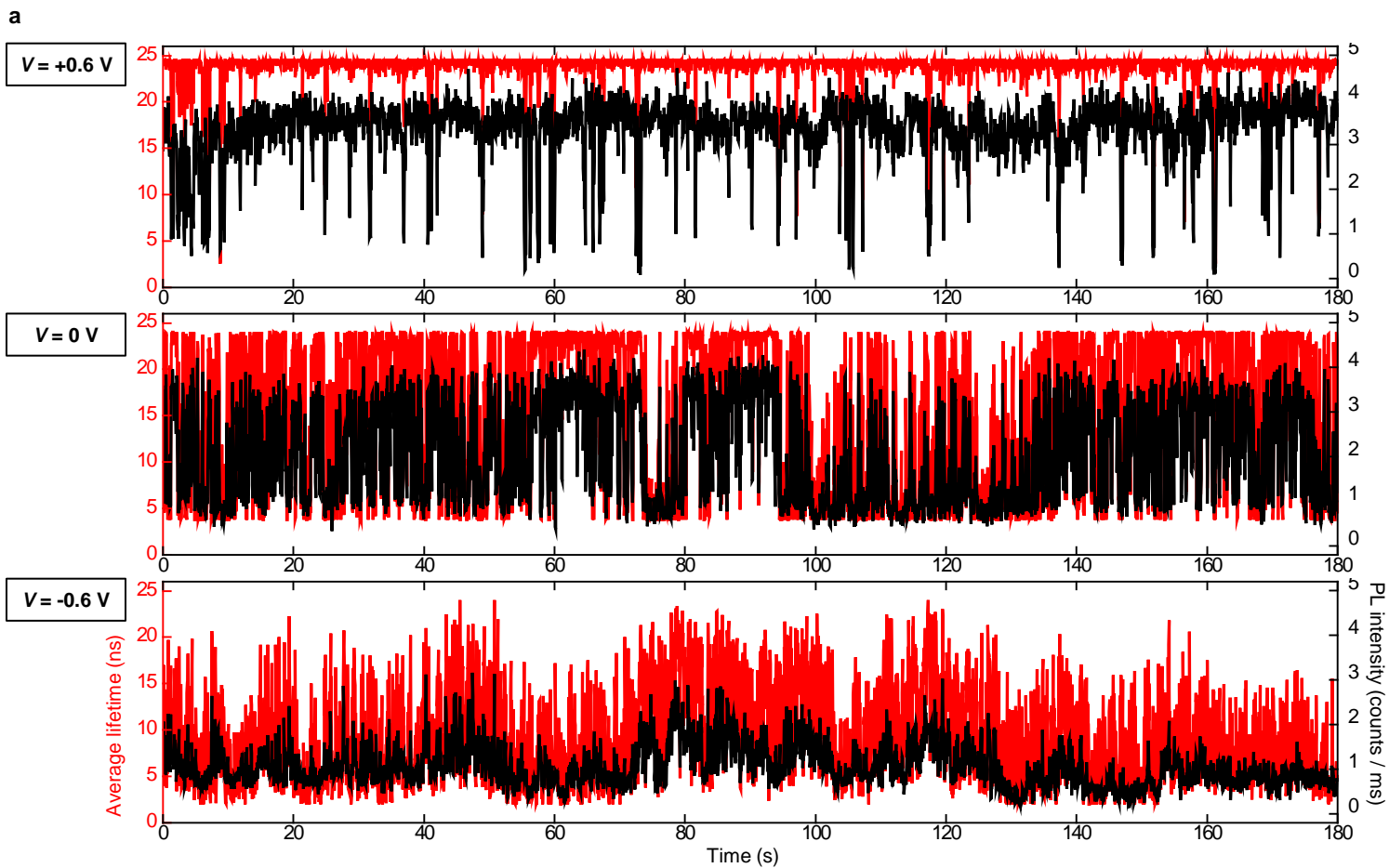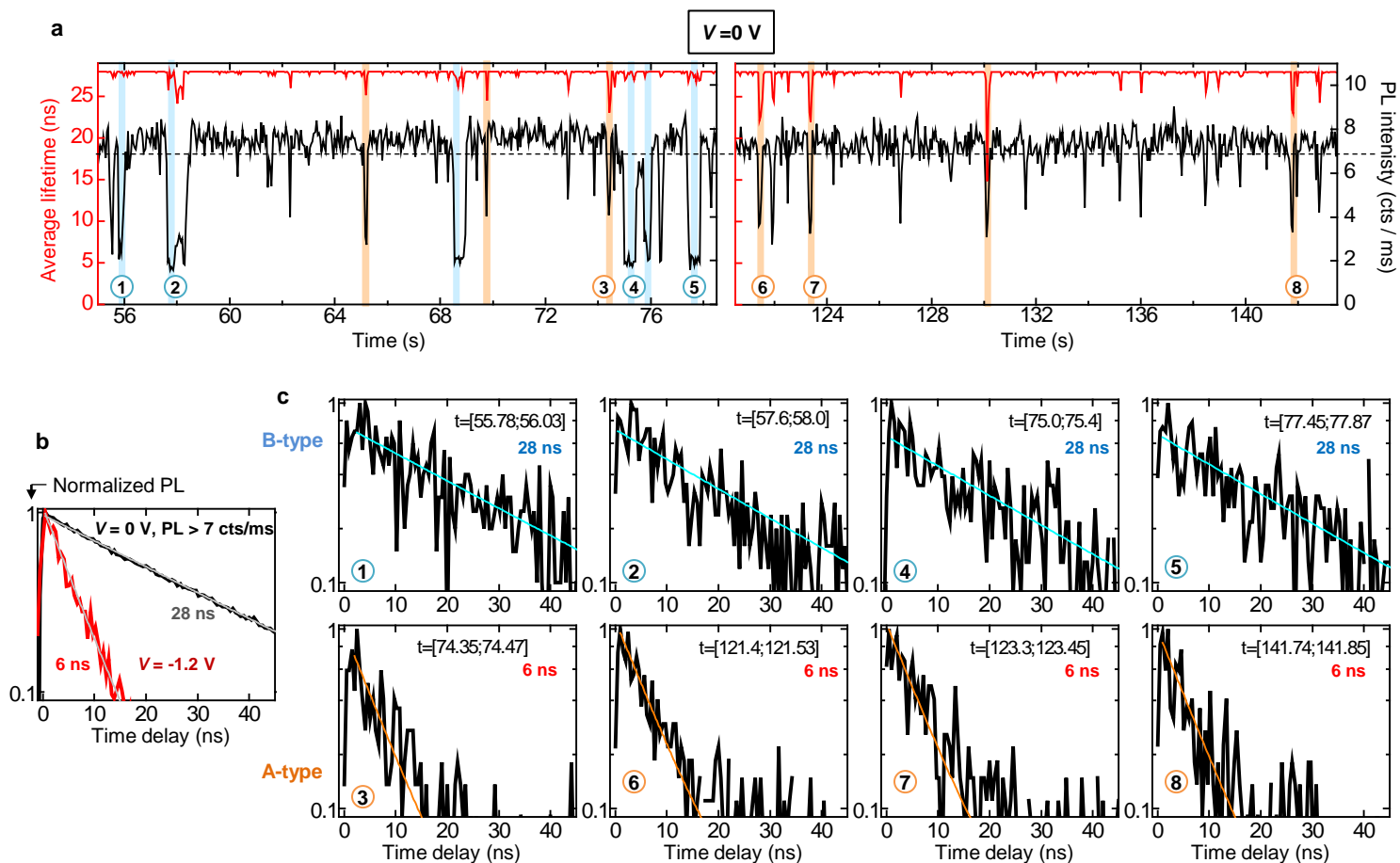
Supplementary Figure 1. Full PL intensity and lifetime trajectories corresponding to Fig. 3 a-b.
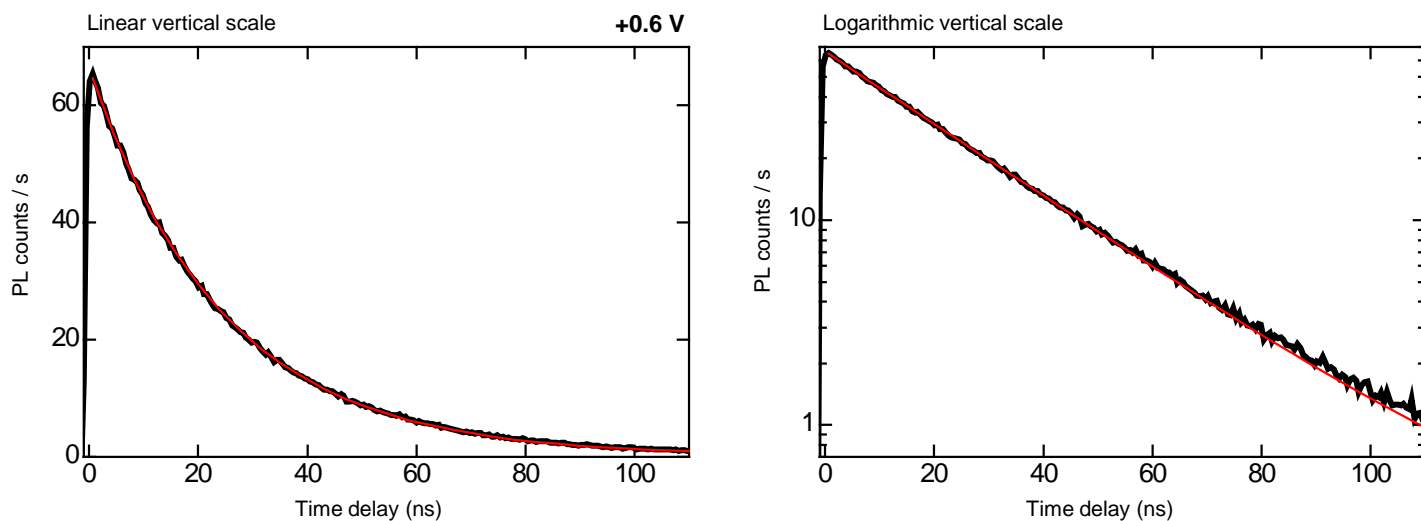
Supplementary Figure 2. Decay curve at +0.6 V for the nanocrystal shown in Fig. 3a.
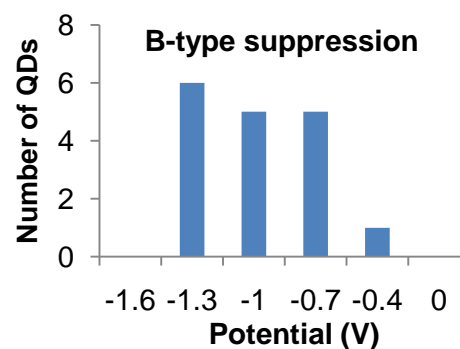
Decay curve at +0.6 V for the nanocrystal shown in Fig. 3a (solid black lines). The red line is a mono-exponential fit with time constant 24 ns, evidencing that the emission is originating exclusively from the neutral exciton.

Supplementary Figure 3. Coexistence of A-type and B-type blinking at 0 V.

a, Two portions of the average PL lifetime (blue) and PL intensity (black) trajectories for the nanocrystal shown in Fig. 4a, at $V = 0$ V. The bin size is 50 ms. Some A-type blinking events are highlighted in orange and are characterized by correlated reduction of intensity and lifetime. In contrast, B-type low-intensity periods (some are highlighted in blue) do not correlate with significant change in average lifetime. **b**, Normalized PL decay curves (logarithmic scale) for the ON state at $V = 0$ V (black, obtained by selecting all bins with intensities higher than the threshold shown as a dashed horizontal line in (a)) and for the same nanocrystal at $V = -1.2$ V (red, no threshold). Thin grey lines are mono-exponential fits, with lifetimes 28 ns at $V = 0$ V and 6 ns $V = -1.2$ V, which can be attributed to X^0 and X^-, respectively. **c**, Normalized PL decay curves at $V = 0$ V corresponding to the small time intervals (100 to 400 ms) highlighted and numbered in (a). Red lines are simulated mono-exponential decays (not fits) with either of the lifetimes extracted in (b). The dynamics during B-type low-intensity periods (curves 1, 2, 4 and 5) is similar to the bright, neutral exciton X^0. A-type events (curves 3, 6, 7 and 8) show a decay dominated by the charged exciton X^-, in agreement with the charging model.

nanocrystal	batch	shell ML	ligand	electrolyte	At 0 V		Suppressed at potential (V)	
					A-type	B-type	A-type	B-type
1	256L	7	W	TBA		X		-1
2	256L	7	W	TBA	X	X		
3	256L	7	W	TBA	X	X		-1
4	256L	7	W	TBA		X		-1.2
5	256L	7	W	TBA		X		-0.8
6	256L	7	W	TBA		X		-1.4
7	256L	7	W	TBA	X		1	
8	256L	7	W	TBA		X		-1.2
9	256L	7	W	TBA		X		-1
10	256L	7	W	TBA	X	X		-1
11	256L	7	W	TBA		X		-1.2
12	256L	7	W	TBA		X		-1.4
13	256M	8	H	PC		X		
14	256M	8	H	TBA		X		-0.8
15	256M	8	H	TBA	X	X	0.5	-0.8
16	256M	8	H	TBA	X	X		-1.4
17	256L	7	W	Li	X			
18	218C	9	H	TBA	X	X	0.8	-1
19	218C	9	H	TBA		X		
20	218C	9	H	TBA		X		-0.6
21	218C	9	H	Li	X		0.6	
22	218C	9	H	Li		X		-0.6
23	218C	7	W	Li	X	X		-0.4

A only	3
B only	13
A+B	7
Total	23

■ A only ■ A+B ■ B only


B-type suppression

Number of QDs vs Potential (V)

Abbreviations:

• W : Water-solube ligands

• H : Native ligands (soluble in hexane)

• TBA : Tetra-butyl-ammonium Perchlorate in Propylene Carbonate

• Li : Lithium Perchlorate in Propylene Carbonate

• PC : Propylene Carbonate only (no supporting electrolyte)

Supplementary Table 1. Statistics on nanocrystals with intermediate shell thickness (7 to 9 MLs).
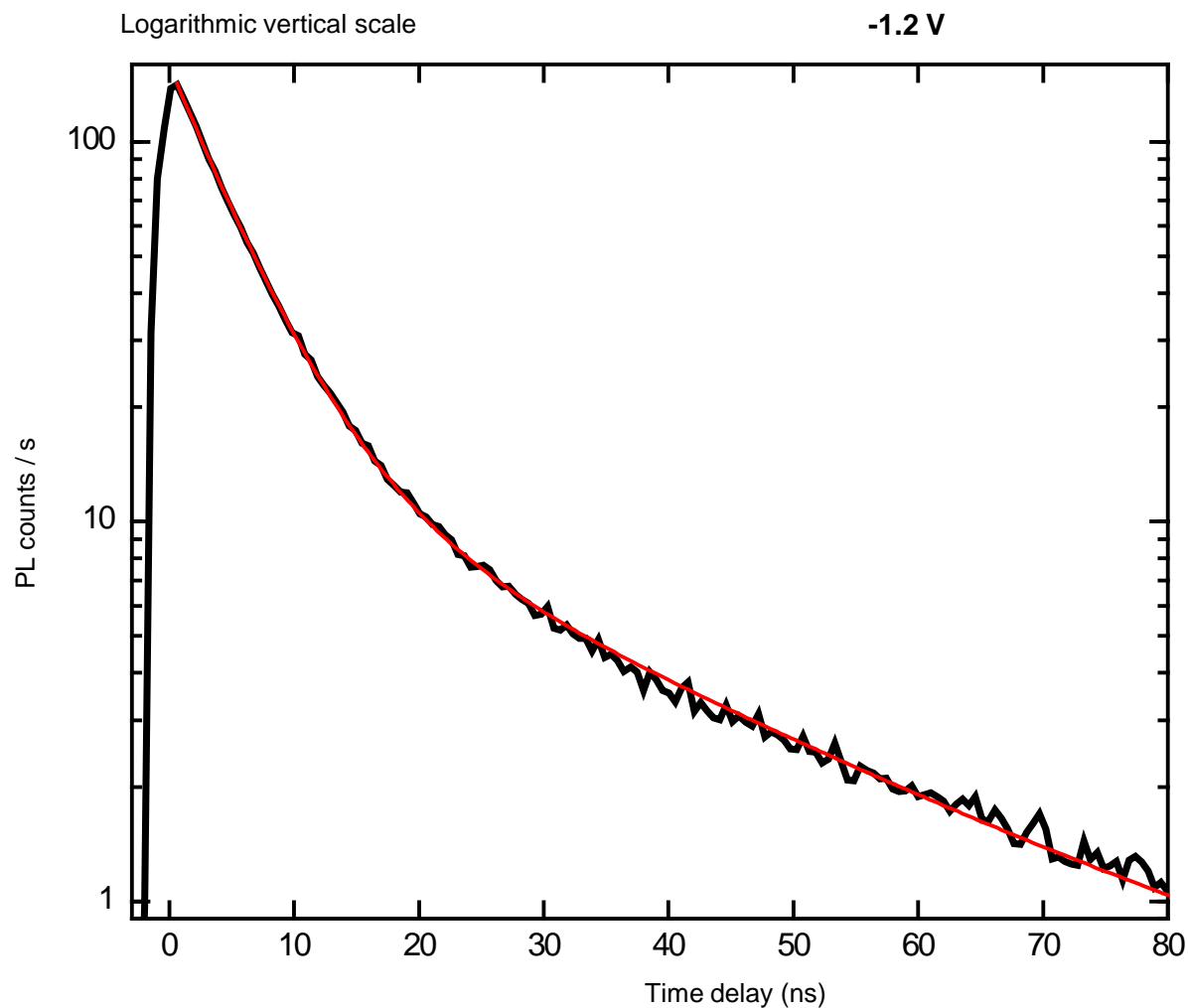
Supplementary Figure 4. Decay curve at -1.2 V for the nanocrystal shown in Fig. 4a.

The PL decay curve (solid black line) for applied potential of -1.2 V for the nanocrystal shown in Fig. 4a. The red line is a biexponential fit with time constants of 6 ns and 28 ns, which yields the average PL lifetime of 12.5 ns seen in Fig. 4a (right). The biexponential decay is a result of very fast switching between the neutral exciton (28 ns lifetime) and the negatively charged trion (6 ns lifetime).
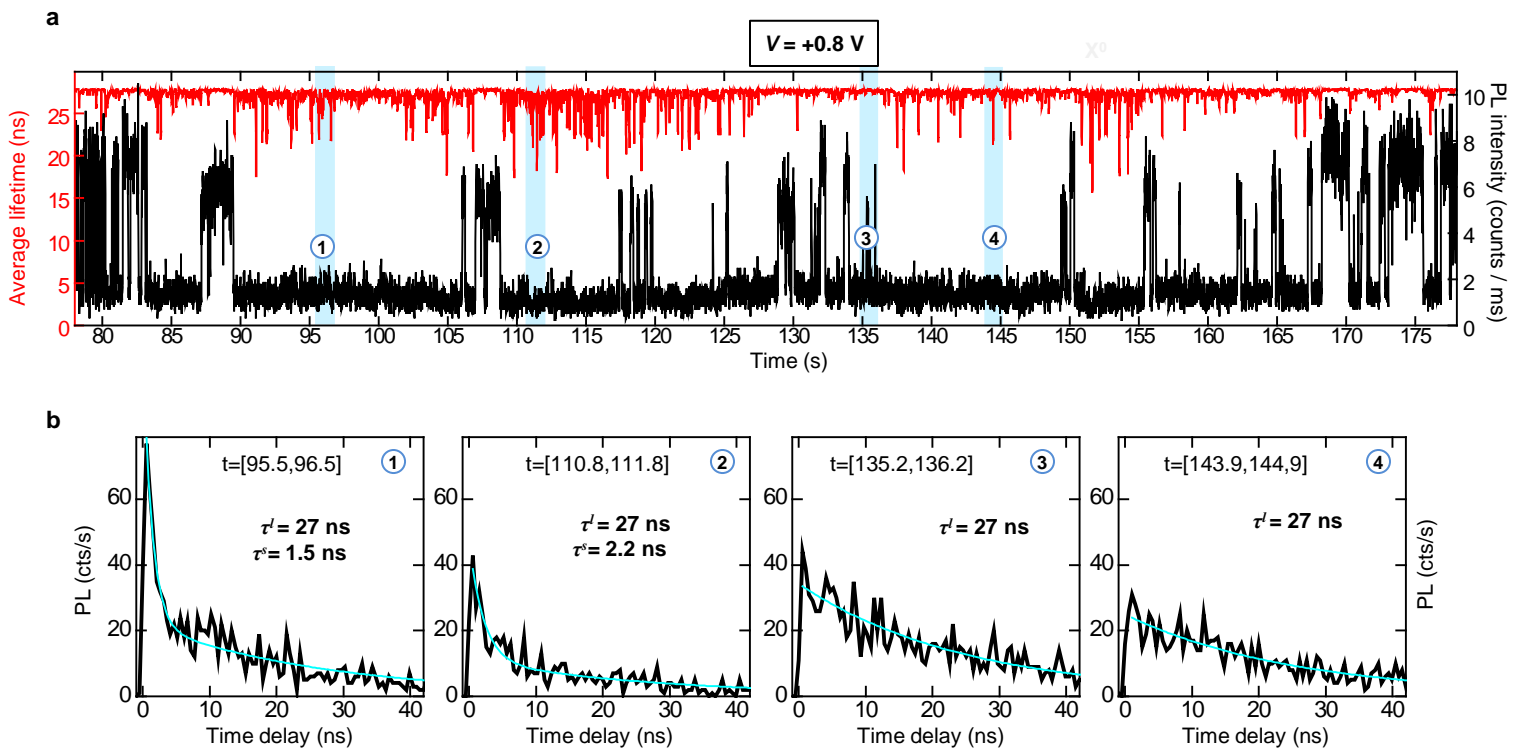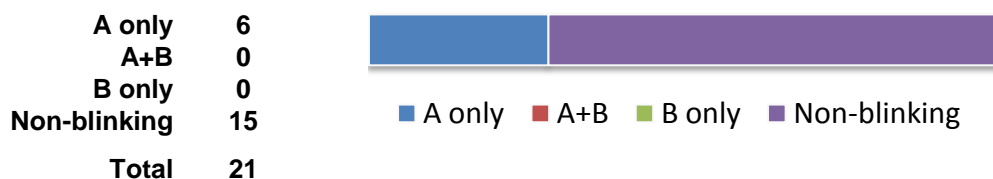
Supplementary Figure 5. Variable PL dynamics within the B-type OFF periods.

a, Portion of the average PL lifetime (blue) and PL intensity (black) trajectories for the nanocrystal shown in Fig. 4a, at $V = +0.8$ V. The bin size is 20 ms. The frequency and length of B-type OFF periods is increased compared to $V = 0$ V. **b**, PL decay curves over 1 s time intervals during OFF periods highlighted and numbered in (a). Thin blue lines are mono- or bi-exponential fits with time constants indicated on the graphs. During most of the OFF periods the decay is quasi-monoexponetial with the lifetime of neutral exciton (~27 ns). But some relatively long intervals like 1 and 2 show an additional fast component of a few nanoseconds. We tentatively attribute this lifetime to positively charged excitons that may form during B-type OFF periods when the captured electrons do not recombine immediately with the hole. The fact that positive trions decay faster than negative trions is not surprising. Auger recombination with excitation of the hole is expected to be more efficient than the processes involving excitation of the electron because the density of valence-band states in II-VI semiconductors is appreciably higher than that of conduction-band states.
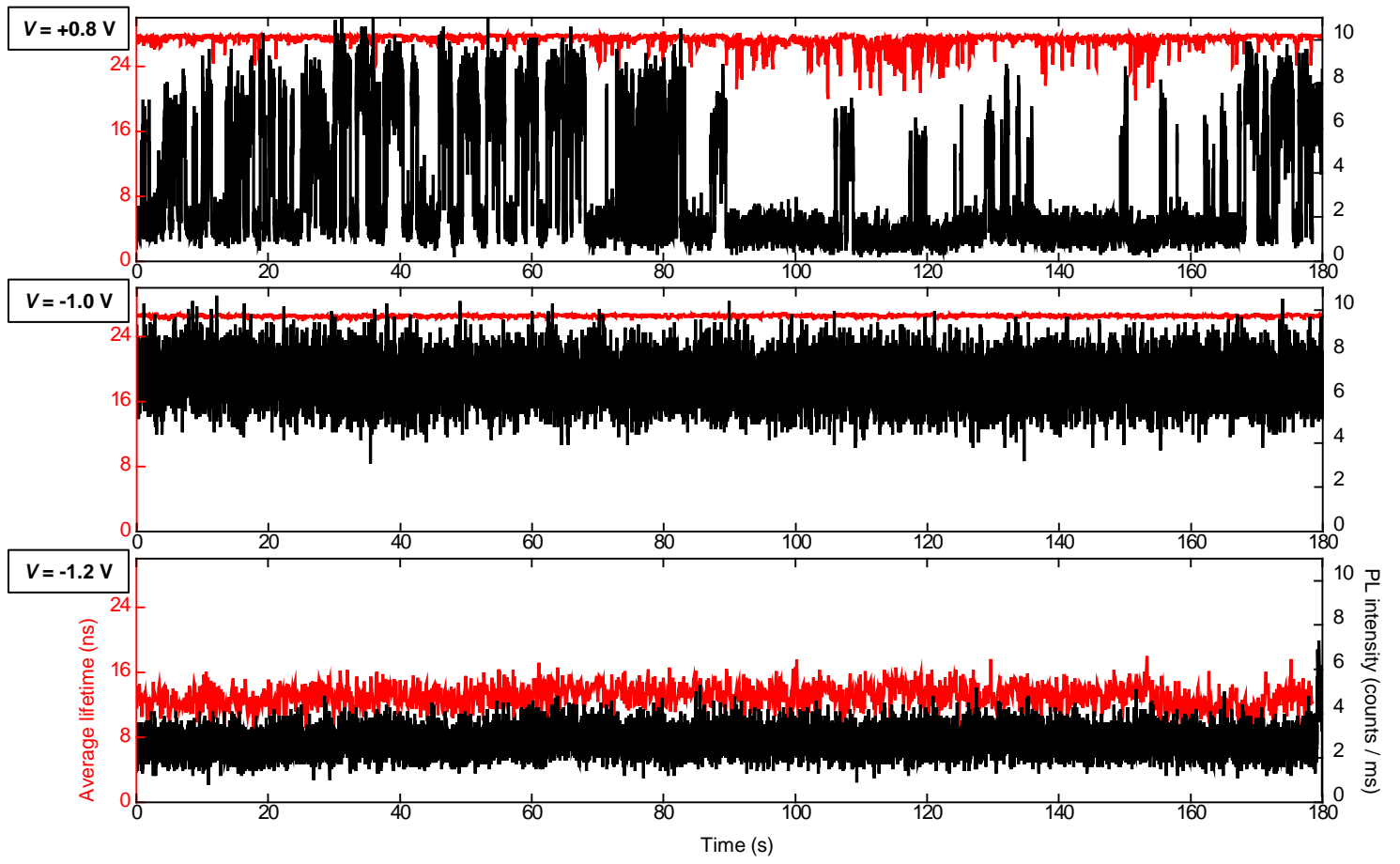
Supplementary Figure 6. Full PL intensity and lifetime trajectories corresponding to Fig. 4a.

nanocrystal	batch	shell ML	ligand	electrolyte	At 0 V		
					Non-Blinking	A-type	B-type
1	216C	15	W	ITO		X	
2	216C	15	W	ITO	X		
3	216C	15	W	ITO	X		
4	216C	15	W	PC	X		
5	216C	15	W	PC	X		
6	216C	15	W	PC	X		
7	216C	15	W	PC	X		
8	216C	15	W	TBA	X		
9	216C	15	W	TBA	X		
10	218C	15	W	Li		X	
11	218C	15	W	TBA	X		
12	218C	15	W	TBA		X	
13	218C	15	W	TBA		X	
14	218C	15	W	Li	X		
15	218C	15	W	Li	X		
16	218C	15	W	Li	X		
17	218C	15	W	ITO		X	
18	218C	15	W	Li		X	
19	218C	15	W	Li	X		
20	218C	15	W	Li	X		
21	218C	15	W	Li	X		

A only	**6**
A+B	**0**
B only	**0**
Non-blinking	**15**
Total	**21**

■ A only　■ A+B　■ B only　■ Non-blinking

Abbreviations:

• W : Water-solube ligands

• H : Native ligands (soluble in hexane)

• ITO : On ITO-coated glass without solvent/electrolyte

• TBA : Tetra-butyl-ammonium Perchlorate in Propylene Carbonate

• Li : Lithium Perchlorate in Propylene Carbonate

• PC : Propylene Carbonate only (no supporting electrolyte)

Supplementary Table 2. Statistics on nanocrystals with thicker shells (~15 MLs).
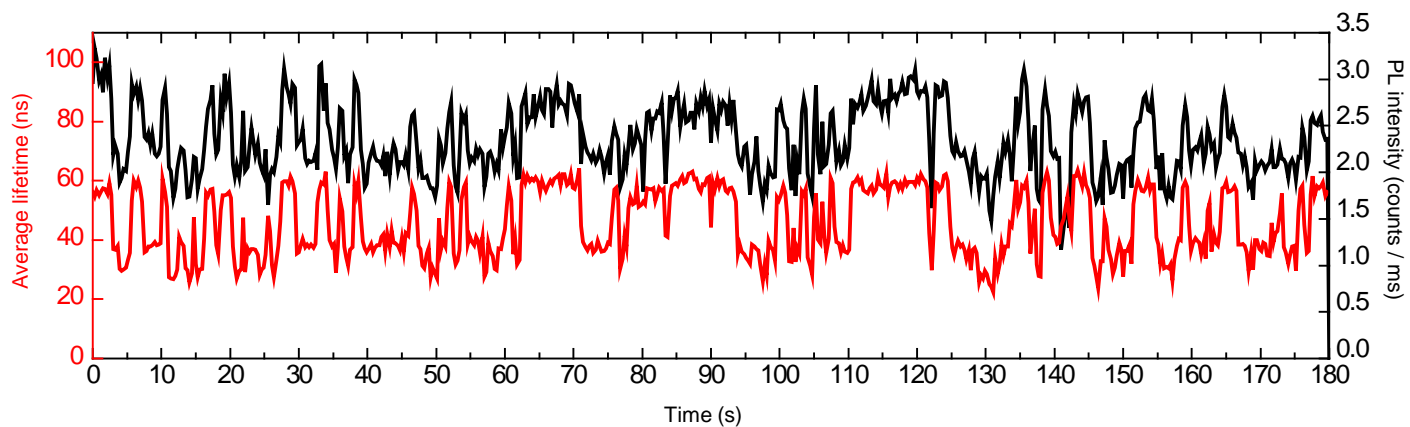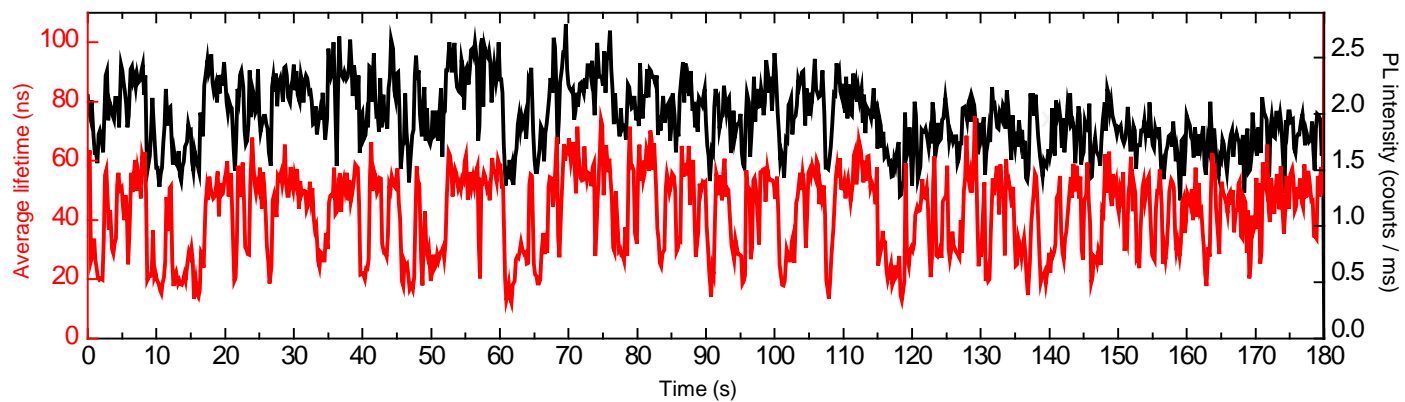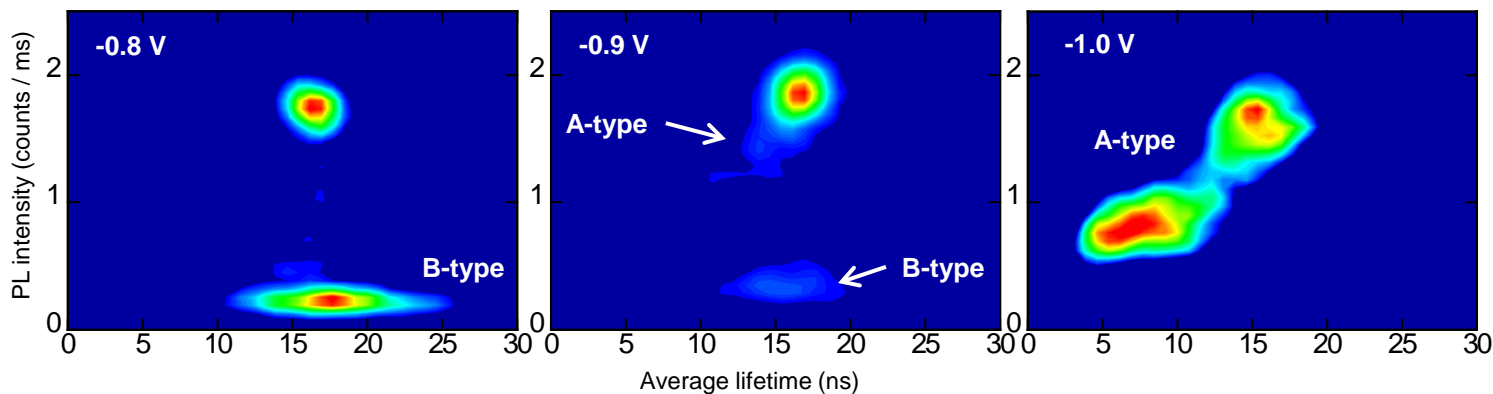
Supplementary Figure 7. A-type blinking in thick shell nanocrystals (15 MLs).

Example of PL lifetime and intensity trajectories for two different 15 ML shell nanocrystals at 0 V, showing only A-type fluctuations. Bin size = 200 ms. The lifetime is evaluated by a weighted average of the micro-time delay for each bin. See also Supplementary Table 2 for complete statistics on 15 ML shell nanocrystals.
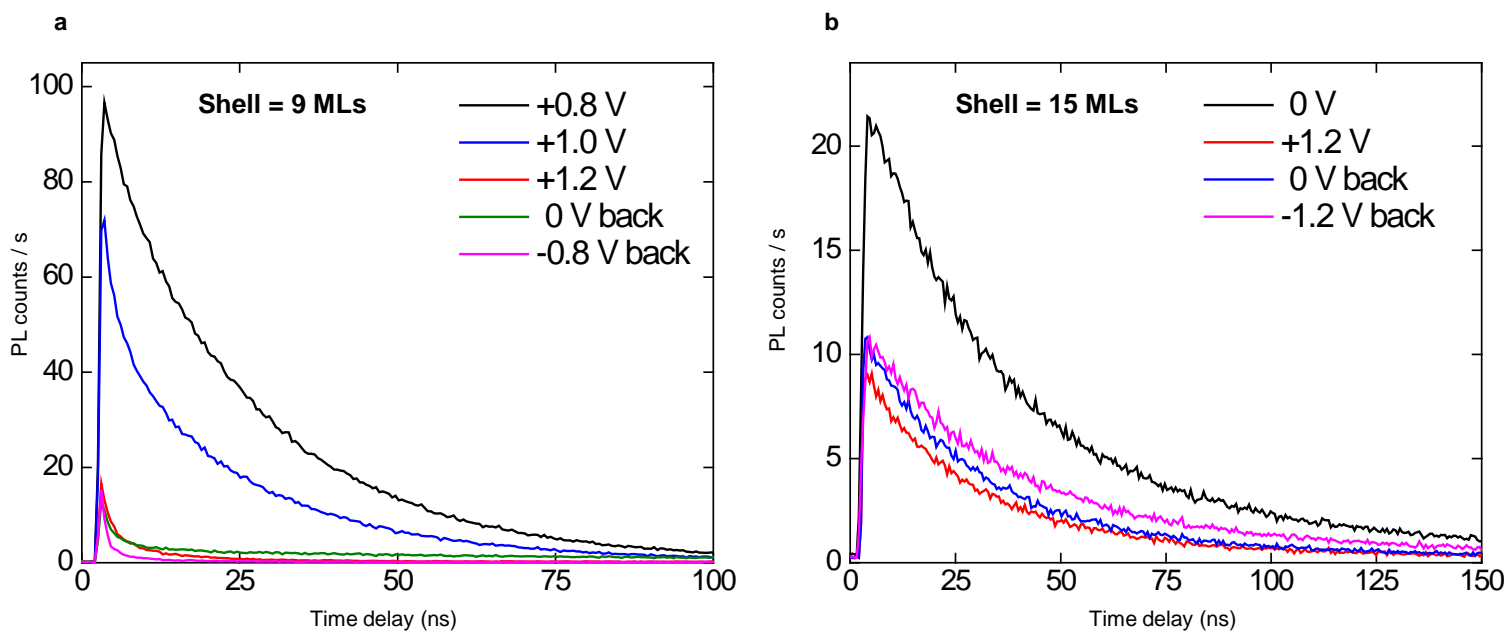
**Supplementary Figure 8. Irreversible quenching at large positive potentials.**

a, Decay curves under increasing positive potential and subsequently back to neutral and negative potential for the nanocrystal shown in Fig. 3 (data shown here taken after the one in Fig. 3). PL is irreversibly quenched by two orders of magnitudes. **b,** Similar experiment on a thicker shell nanocrystal (15 ML). The quenching is also irreversible, but its magnitude is much weaker. This support our arguments for the activation of hot-electron traps at positive potential. This process should indeed be exponentially suppress by increasing the shell thickness because of the reduction of the wavefunction overlap with the surface states. In addition, more experiments on 15-ML shell nanocrystals have shown the absence of B-type blinking under neutral potential in all the nanocrystals we studied. (see Supplementary Table 2 and Supplementary Figure 8).

Supplementary Figure 9. Another example of A/B-type blinking control by electrochemical potential.

FLIDs from a nanocrystal with 7 MLs CdS shell in water-soluble ligands (see Methods) at three different potentials. At -0.8 V, the nanocrystal is in a strong B-type blinking regime. At -0.9 V B-type events are much less frequent but A-type fluctuations appear.. At -1.0 V, blinking is completely A-type (fluctuations between the neutral and negatively charged exciton).

These FLIDs were constructed using a bin size of 20 ms. For each bin the PL lifetime was calculated by a weighted average of the decay histogram ("micro-times" values). This method does not rely on a fitting procedure but gives results similar to the one presented in Fig. 3 and 4, thus confirming the robustness of our analysis. The main limitation here is that no offset can be accounted for before evaluating the lifetime. Therefore the flat background due to dark counts leads to an overestimate of the lifetime when PL counts are low, as in the B-type state at -0.8 V.
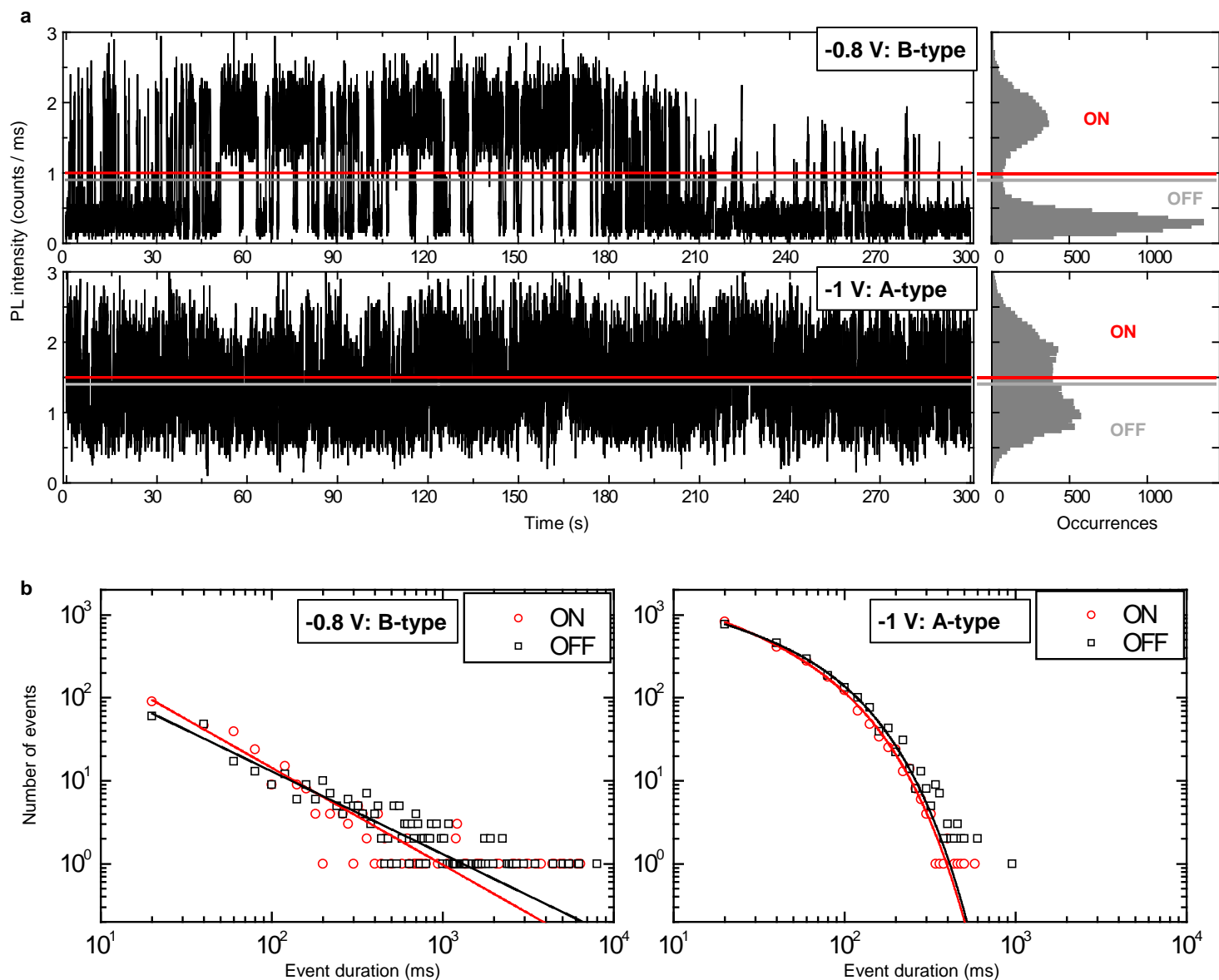
**Supplementary Figure 10. Different statistics for A vs. B-type ON/OFF times in the same nanocrystal.**

a, PL intensity time trace and occurrence histogram for the nanocrystal shown in Suppl. Fig. 9 at two different potential at which the nanocrystal is either in B-type (-0.8 V) or A-type (-1 V) blinking mode. The bin size is 20 ms. **b,** Corresponding probability densities of ON (red circles) and OFF (black squares) event durations. The thresholds are indicated in (**a**) by red (ON) and grey (OFF) lines. The data at -0.8 V are fitted by pure power laws with exponents -1.17 (ON, red line) and -1.00 (OFF, black line). At -1 V, we need to introduce an exponential cut-off to the power law to fit the experiment. The exponent are -0.54 (ON, red line) and -0.37 (OFF, black line), whereas the cut-off times are 73.4 ms (ON) and 70.8 ms (OFF). The qualitative difference in the ON/OFF times statistics for A and B-type blinking in the same nanocrystal highlights the fundamentally distinct nature of their mechanisms.
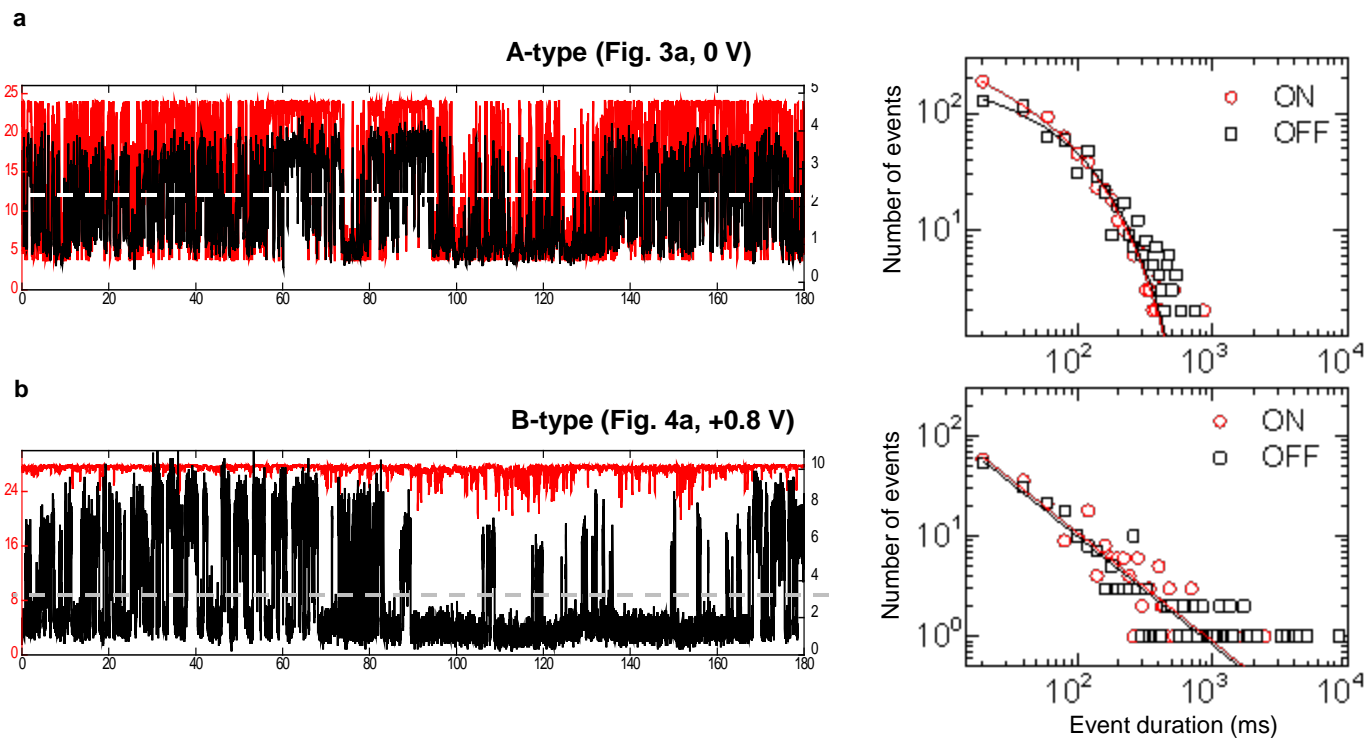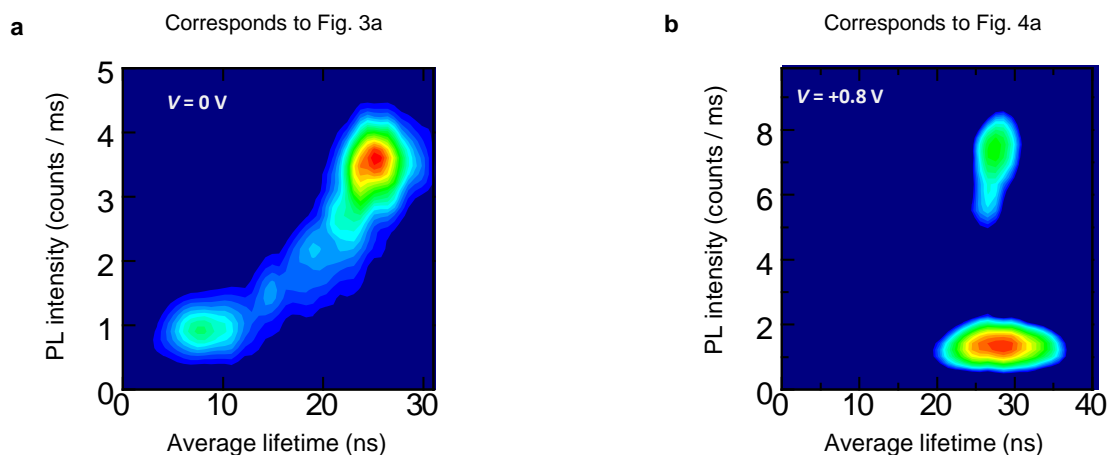
Supplementary Figure 11. ON/OFF times statistics for the nanocrystals in Figs 3 and 4.

a, PL time trace and corresponding ON/OFF event duration statistics for the nanocrystal in Fig. 3a at 0 V showing exclusively A-type blinking. The best fits (solid lines) are obtained with exponents -0.42 (ON) and -0.20 (OFF), and exponential cutoff times 111.5 ms (ON) and 104.6 (OFF). **b,** Same analysis on the nanocrystal of Fig. 4a at +0.8 V, showing only B-type blinking. The solid lines are the best fitted pure power laws with exponents 1.08   0.02 (both ON and OFF). All statistics were calculated with a 20 ms bin; the thresholds discrimating OF/OFF levels are displayed on the time traces on the left.
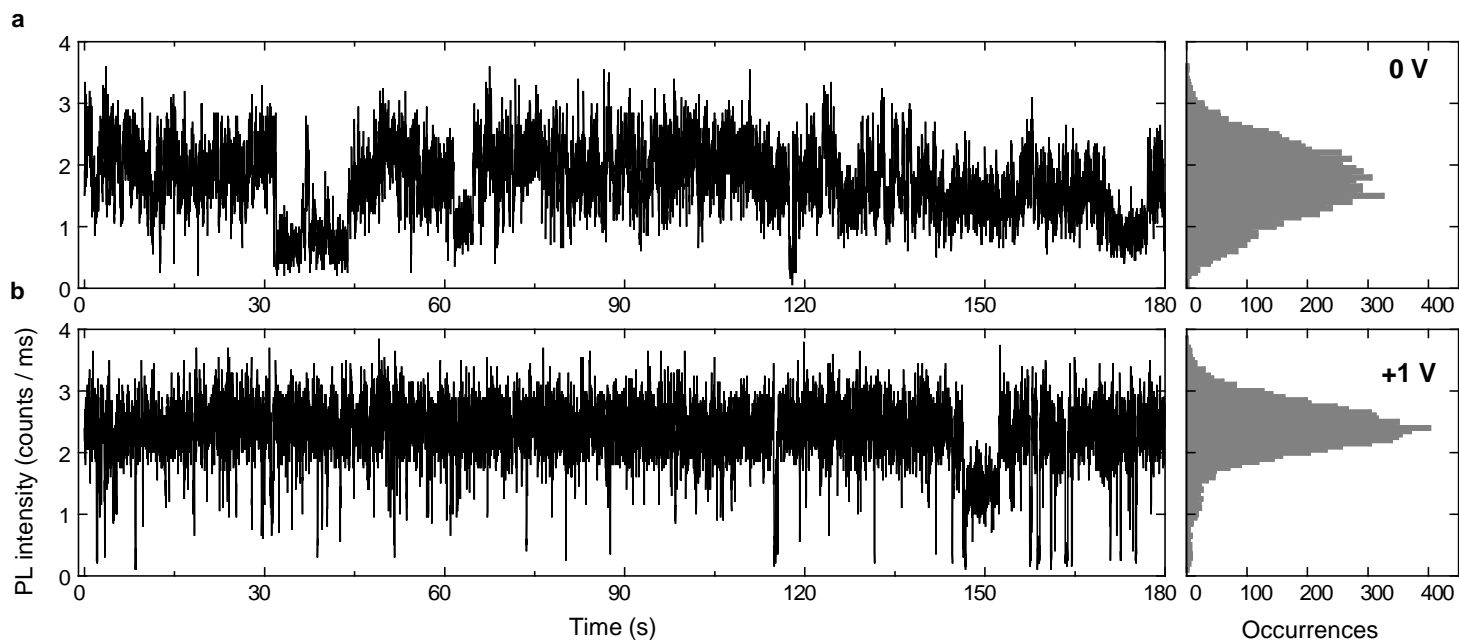
Supplementary Figure 12. An example of A-type flickering suppressed at +1 V.

PL intensity time trace and corresponding distribution histogram at 0 V **(a)** and +1 V **(b)**, showing that fast A-type fluctuations can be significantly reduced under positive potential. The binning time is 20 ms. The nanocrystal is number 7 in Supplementary Table 1.

a Corresponds to Fig. 3a

V = 0 V

PL intensity (counts / ms)

Average lifetime (ns)

b Corresponds to Fig. 4a

V = +0.8 V

PL intensity (counts / ms)

Average lifetime (ns)

Supplementary Figure 13. Validity and robustness of the fitting procedure used in the main text to identify A- and B-type blinking.

FLIDs from the nanocrystals presented in (**a**) Fig. 3a and (**b**) Fig. 4a re-constructed with a "weighted average" lifetime algorithm. As explained in Supplementary Fig. 9, for each time bin, we evaluate the PL lifetime by calculating a weighted average of PL photon arrival times . This method does not rely on any fitting procedure. Importantly, it yields results that are similar to those presented in the main text. This supports the validity of the multiexponential approach used in the present study.